Hot-core characterization of direct-drive spherical cryogenic D$_2$ target implosion

V. A. Smalyuk, J. A. Delettrez, S. B. Dumanis,[a)] R. Epstein, V. Yu. Glebov,
D. D. Meyerhofer,[b)] P. B. Radha, S. P. Regan, T. C. Sangster,
C. Stoeckl, and N. C. Toscano[c)]
Laboratory for Laser Energetics, University of Rochester, 250 East River Road, Rochester,
New York 14623

J. A. Frenje, C. K. Li, R. D. Petrasso,[d)] and F. H. Séguin
Plasma Science and Fusion Center, Massachusetts Institute of Technology, Cambridge,
Massachusetts 02139

J. A. Koch
Lawrence Livermore National Laboratory, Livermore, California 94551

A novel model to infer the hot-core temperature–density profiles in cryogenic deuterium capsule implosions is presented. The profiles are consistent with the measured primary deuterium–deuterium and secondary deuterium–tritium yields, the neutron-averaged ion temperature, and the x-ray image at peak neutron production. The electron pressure and the areal density of a neutron-producing region were inferred to be 2.7 ± 0.4 Gbar and ~ 10 mg/cm^2, respectively. This new model introduces a more accurate hot-core characterization from previous techniques. © *2005 American Institute of Physics*. [DOI: 10.1063/1.1919427]

I. INTRODUCTION

In inertial confinement fusion[1] (ICF), a spherical shell is irradiated either directly by a large number of overlapping laser beams (direct drive) or by x rays produced in a high-Z "hohlraum" (indirect drive).[2] During the laser-driven acceleration phase of an implosion, the target compresses while it converges, then decelerates to peak compression as the core is heated to high temperatures, causing a thermonuclear burn within its fuel. The current goal of ICF research is to achieve ignition and positive gain, where the amount of energy released through thermonuclear fusion is higher than the amount of laser energy used to drive the target. The combination of high temperature and areal density (ρR) in the compressed fuel is necessary to ignite the target.[2] This goal is expected to be achieved at the National Ignition Facility (NIF),[2] currently under construction. In the direct-drive ignition target design[3] for the NIF, a 3.4-mm-diameter, 350-μm-thick cryogenic deuterium–tritium (DT) shell is imploded with 192 overlapped laser beams with a total energy of 1.5 MJ. The fusion energy will be released through the nuclear reaction D+T$\rightarrow$^{4}He(3.5 MeV)+n(14.1 MeV). The expected neutron yield of 2.5×10^{19} (corresponding to a gain of ~ 45) will be achieved at a fuel temperature of ~ 30 keV and an areal density of ~ 1200 mg/cm^2 at peak compression.

While cryogenic DT targets will be used for fusion ignition, the current implosion program on the 60-beam, 351-nm Omega laser system[4] uses cryogenic D$_2$ targets to study the relevant implosion physics. The D$_2$ targets are similar to DT targets, but simpler to produce and more useful for diagnosing target conditions near peak compression. The primary fusion reaction in D$_2$ fuel has two branches: (a) D+D $\rightarrow$^{3}He (0.82 MeV)+n(2.45 MeV), and (b) D+D $\rightarrow$T(1.01 MeV)+p(3.02 MeV). The primary reaction product T reacts with D through the secondary reaction D +T(0–1.01 MeV)$\rightarrow$^{4}He+n(11.9–17.2 MeV). Early experiments[5,6] with cryogenic targets used the size of the core emission and the ratio of secondary DT to primary deuterium–deuterium (DD) neutron yields to estimate target compression. This technique was first used by Azechi *et al.*[7] and by Cable and Hatchett.[8] In their calculations, the core ρR was inferred from the secondary to primary yield ratios, assuming the core had a uniform temperature and density. For more than two decades, ICF implosions had been typically characterized by the measured neutron yields, neutron-averaged ion temperatures, and areal densities inferred using yield ratios based on simplified core models. For the success of ICF, it is necessary to infer core temperature–density profiles and directly compare them with hydrocode simulations. Because the target ignition designs are based on hydrocode predictions, they should be benchmarked by the most comprehensive set of measurements.

Recently Radha *et al.* modeled[9] core temperature–density profiles at peak neutron production in plastic-shell targets. About ten different experimental observations with several different types of targets (having various dopants in a gas fuel and plastic shell) were necessary for a comprehensive characterization of the core conditions.[9] Kurebayashi *et al.*[10] used secondary particles (neutrons and protons) to study their usefulness for hot-core modeling of plastic and cryo-

---

genic capsules. Cable *et al.*[8,11] used the shape of the measured secondary neutron spectrum to constrain core conditions. The cryogenic D_2 targets cannot have dopants, but because they are much simpler (there is no complication of mixing of the different materials in the core), it is possible to characterize them (with the same level of detail as plastic shells) with fewer experimental observables. This Letter describes experiments where measured primary DD and secondary DT neutron yields, neutron-averaged ion temperatures, and x-ray images at peak neutron production are used to infer the electron-pressure and temperature–density profiles in cryogenic D_2 implosions for the first time. The areal densities of neutron production and "triton-stopping" regions are introduced to characterize target compression. These compression measurements are significant improvements over the ρR inferred from the secondary- to primary-yield ratios solely. Because they are derived from the temperature–density profiles consistent with experimental measurements, they provide more accurate measurements of compression. The established way to characterize implosions in ICF is to compare measured and predicted neutron data such as primary and secondary neutron yields and ion temperatures. This article shows that even though a simulation or a model can predict all neutron data in exact agreement with the experiment, it still could have significant uncertainty in the main compression parameters such as core pressure and hot-spot areal density. The model introduced in this article allows comprehensive hot-core characterization with core temperature–density profiles and it dramatically reduces the uncertainties of hot-core compression. If, in addition, the energy spectrum of the secondary neutrons[8,11] was measured, it would give additional constraint to the present model, potentially decreasing the uncertainty of inferred core conditions.

II. EXPERIMENTAL CONFIGURATION

The experiments were direct-drive implosions of ~ 920-μm-initial-diameter targets with shells that consisted of ~ 100-μm-thick inner D_2-ice layers and outer 5-μm-thick plastic CD layers.[12] The targets were imploded with a 1-ns square pulse shape with a total on-target energy of ~ 23 kJ on the 60-beam Omega laser system.[4] The laser beams were smoothed with distributed phase plates,[13] 1-THz two-dimensional smoothing by spectral dispersion,[14] and polarization smoothing[15] using birefringent wedges. The measured experimental yield ratios relative to those predicted using one-dimensional (1D) simulations were typically $\sim 30\%$ in a large number of similar implosions. In one implosion, the experimental yield was closer to the predicted yield (59%); therefore, this implosion was used for the analysis presented here. This stable implosion was used to demonstrate the accuracy of the modeling based on neutron and x-ray data before applying it to more-unstable implosions. The measured primary DD and secondary DT neutron yields for this implosion were $Y_1 = (1.24 \times 10^{11}) \pm (8 \times 10^8)$ and $Y_2 = (1.17 \times 10^9) \pm (3 \times 10^7)$, respectively.[12] The measured neutron-averaged ion temperature was $T_i = 3.6 \pm 0.5$ keV and the neutron burn width was $\tau = 170 \pm 25$ ps.[12] The core images[12] were measured with an

x-ray framing camera with a spatial resolution of ~ 10 μm, a temporal resolution of ~ 40 ps, and a 200-μm-thick beryllium filter (which transmitted x rays with energies of more than ~ 2 keV).

III. ANALYSIS TECHNIQUE AND EXPERIMENTAL RESULTS

The target core conditions at peak neutron production were inferred by choosing temperature $[T(\mathbf{r})]$ and density $[n(\mathbf{r})]$ profiles that produced the same primary and secondary neutron yields, the neutron-averaged ion temperature (calculated the same way as in Ref. 9), and the size of x-ray images as measured within experimental uncertainties. In the first stage of modeling, only those temperature–density profiles that were consistent with the primary DD neutron yield and neutron-averaged ion temperature were selected from all possible combinations at a particular electron pressure (the hot core was assumed to be isobaric). In the second stage, profiles consistent with the secondary DT neutron yield were chosen from those selected in the first stage. Similarly, the temperature–density profiles consistent with all neutron measurements were chosen at each electron pressure in the range of $1 - 10$ Gbar. Finally, only those temperature–density profiles that were consistent with the size of the x-ray core images were chosen to characterize the hot core at peak neutron production. The following assumptions were used in the core modeling: (1) The core plasma was a fully ionized ideal gas (the analysis of more-compressed implosions in the future will include degeneracy effects[9]), (2) the core was isobaric $[P_e(\mathbf{r}) = \text{const}]$ at stagnation, (3) the temperature–density profiles were spherically symmetric, (4) the electron and ion temperatures and densities were equal, (5) the core was static during the time of neutron production τ therefore, the inferred pressure and temperature–density profiles were considered to be neutron averaged, and (6) the temperature decreased monotonically from the center. Li and Petrasso's plasma-stopping powers[16] were used to calculated triton energy loss as it propagates in a three-dimensional (3D) core for the secondary DT neutron-yield calculations. The x-ray images were constructed using radiation-transport calculations in a fully ionized deuterium plasma with free-free emission and absorption.[17]

Figure 1(a) shows one of the grids used to construct temperature profiles. The temperature step was 250 eV and the distance step was 20 μm (distance steps of 15, 10, and 5 μm were used in additional, more-detailed grids). Using grids with finer spatial resolution resulted in the same answers as shown in Fig. 1. The curves show examples of two (out of nearly $\sim 10^{10}$) temperature profiles $T(\mathbf{r})$ used in the modeling. The corresponding density profiles $n(\mathbf{r})$ were calculated using $P_e(\mathbf{r}) = n(\mathbf{r}) \times T(\mathbf{r})$. The range of temperatures that satisfy the measured DD neutron yield and neutron-averaged ion temperature (calculated in the first stage of modeling) is shown by the lightly shaded region in Fig. 1(b) at an electron pressure of 2.6 Gbar. The results of the second stage of modeling—the temperature profiles consistent with secondary DT neutron yield (in addition to primary DD yield and neutron-averaged ion temperature)—are shown by the
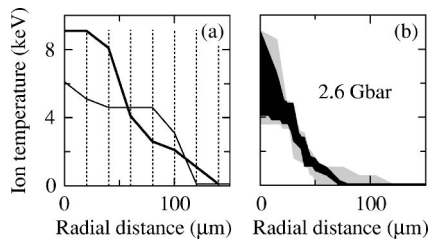
FIG. 1. (a) The temperature-radius grid. The temperature step is 250 eV, and the radial distance step is 20 μm, as shown by the vertical dotted lines. The thick and thin solid lines show examples of monotonically decreasing temperature profiles as a function of the radial distance used in core modeling. (b) The range of ion-temperature profiles consistent with the measured primary DD yield and neutron-averaged ion temperature (lightly shaded area), and in addition, the secondary DT yield (darkly shaded area), at an electron pressure of 2.6 Gbar.

FIG. 3. (a) X-ray framing camera image of the core at peak neutron production (upper left side); the horizontal and vertical lineouts of this image (thick and thin lines). The shaded area lies in between the lineouts of the calculated images at electron pressures of 2.3 and 3.1 Gbar. All lineouts are normalized to the integrated intensities under the curves. The range of (b) core temperature and (c) density profiles corresponding to electron pressures in the range from 2.3 to 3.1 Gbar, which produce sizes of x-ray emission consistent with that of the measured x-ray image (shown by gray areas). The 1D LILAC predictions are shown by the dashed lines.

darkly shaded region. Similar calculations were conducted for electron pressures in the range from 1 to 10 Gbar. As an example, the ranges of temperature profiles consistent with all neutron measurements for three different electron pressures (1.3, 2.6, and 5.2 Gbar) are shown in Fig. 2(a). It was found that for any electron pressure above 1.3 Gbar, temperature-density profiles consistent with all neutron measurements could be found. The neutron measurements by themselves are not sufficient to accurately characterize the target core pressure and other compression parameters at peak neutron production with uncertainty in the pressure at least an order of magnitude. The profiles at different pressures, however, would make different sizes of x-ray emission, as can be seen from the profiles shown in Fig. 2(b). Therefore, for various temperature-density profiles, the x-ray images were constructed and compared with the one measured at peak neutron production. In these calculations, the transmission of the Be filter and the x-ray spectral response of the framing camera gold photocathode were taken into account. The size of the x-ray image is very sensitive to the core pressure [see Fig. 2(b)]. The measured core image at peak neutron production is shown in Fig. 3(a). Figure 3(a) also shows two central lineouts of the measured image in horizontal and vertical directions by thick and thin solid lines. The image is slightly elliptical with full widths at half maximum (FWHM's) ranging from about 94 to 100 μm in two perpendicular directions. The measured image is consistent with calculated images in the electron-pressure range

from 2.3 to 3.1 Gbar. The shaded area in Fig. 3(a) is between the 2.3- and 3.1-Gbar lineouts, and the measured lineouts lie within this area. The ranges of inferred core temperature and density profiles, corresponding to this range of electron pressures, are shown in Figs. 3(b) and 3(c), respectively. As a result, only a relatively narrow range of temperature—density profiles is consistent with all neutron and x-ray measurements simultaneously. It is important to note that the novel aspect of this work, the inclusion of the x-ray size of the core, has reduced the uncertainty in the inferred pressure from an order of magnitude to ∼20%. The dashed curves correspond to simulations using the 1D hydrocode LILAC,[12] that are discussed below.

Even though temperature-density profiles contain all the information about the core conditions the core ρR has always been a simple and useful measurement[7,8] of target performance in ICF. Modeling based on flat temperature-density profiles[7,8] allows only estimates of the areal density. Detailed temperature-density profiles consistent with all neutron and x-ray measurements are required for accurate determination of the core ρR. The solid line in Fig. 4(a) shows a cumulative DD neutron yield as a function of the core areal density, calculated using temperature-density profiles at an electron pressure of 2.6 Gbar. The cumulative yield is the radial integral of the radial neutron production, while areal density is a radial integral of the density. The ρR of the "burn" region of ∼10 mg/cm^2 was defined at 95% of the maximum value of the cumulative yield. The burn region ρR inferred from the temperature-density profiles at 1.3 Gbar [see Fig. 2(a)] is a factor of 2 smaller. Even though the 1.3-Gbar profiles are consistent with all neutron measurements, they were rejected because they did not predict the measured x-ray images. This means that the core ρR inferred solely from the yield ratio of primary to secondary neutrons (especially using flat profiles that are not consistent with the measurements) could be very
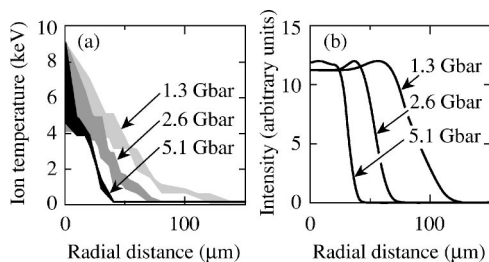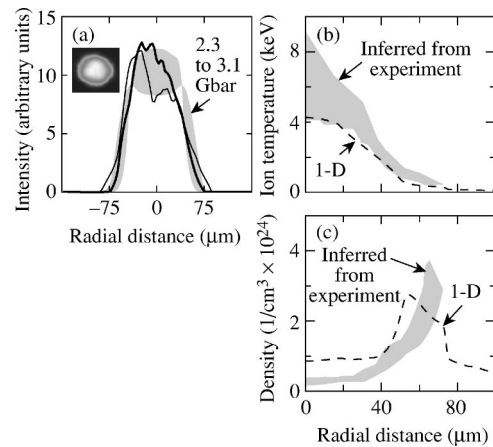

FIG. 2. (a) The range of temperature profiles that satisfy measured primary DD, secondary DT yields, and neutron-averaged ion temperature, calculated for electron pressures of 1.6 (light), 2.6 (medium), and 5.1 Gbar (darkly shaded area). (b) Examples of x-ray radial lineouts (normalized to their highest values) calculated for the same pressures of 1.6, 2.6, and 5.1 Gbar.
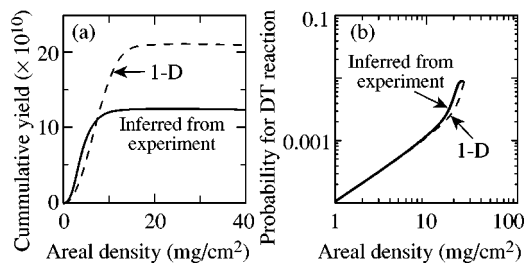
FIG. 4. (a) Cumulative yields as a function of core ρR, inferred from the experiment, for an electron pressure of 2.6 Gbar (solid curve) and from a 1D simulation (dashed curve). The ρR's of the "burn" regions (~ 10 and ~ 15 mg/cm^2, respectively) were defined at 95% of the maximum value of the cumulative yield. (b) Probability for a secondary DT reaction (equal to a ratio of DT to DD yields) as a function of core ρR, calculated for an electron pressure of 2.6 Gbar (solid curve). The triton probes a core ρR of ~ 23 mg/cm^2 before being stopped in the core. The dashed curve corresponds to a 1D simulation with a "triton-stopping" ρR of ~ 27 mg/cm^2.

inaccurate. The total target ρR was measured to be ~ 61 mg/cm^2 at peak neutron production using a downshift in the secondary proton spectra.[10]

The ρR of a triton-stopping region is another useful parameter describing the extent of the hot core that is probed by the neutron measurements. The tritons are born in the neutron-producing region through the DD fusion reaction. They are slowed down and stopped while they move through the compressed target.[16] The triton-slowing rate depends on plasma temperature and density: it is higher in colder, less-dense plasmas;[7,8] therefore, the ρR of a triton-stopping region (or the ρR necessary to stop the triton) is higher in hotter, denser cores. As the triton propagates in the core, it can react with deuterium through a secondary DT reaction, producing a secondary DT neutron.[7,8] Figure 4(b) shows (by a solid line) the probability for the DT reaction as a function of the core areal density, calculated for the same conditions as in Fig. 4(a) at an electron pressure of 2.6 Gbar. In this calculation, the triton is born at the center and propagates toward the outer surface until it is stopped after probing ~ 23 mg/cm^2 of the core plasma. The probability for the DT reaction dramatically increases right before the triton is stopped because the DT-reaction cross section increases as the triton slows down in the plasma. Therefore, the secondary DT neutron yield is very sensitive to the temperature–density profiles in the outer part of the hot core, while the primary DD yield is more sensitive to conditions in the central part of the core.

The modeling results were compared with the predictions[12] of a 1D LILAC simulation (dashed lines in Figs. 3 and 4). The predicted DD neutron yield of 2.1 $\times 10^{11}$ was close to the measured yield of 1.24×10^{11}, while the simulated neutron-averaged ion temperature of 3.1 keV was a little lower than the measured 3.6 keV. As a result, the simulated temperature profile [see Fig. 3(b)] was a little lower than the temperature range inferred from the experiment, while the density profile was a little higher [see Fig. 3(c)]. In the 1D simulation, the burn and triton-stopping region ρR's were very close to those inferred from the experiment. In the simulation, the burn ρR was ~ 15 mg/cm^2 (~ 10 mg/cm^2 in the experiment) and the triton-stopping re-

gion ρR was ~ 27 mg/cm^2 (~ 23 mg/cm^2 in the experiment), as shown in Fig. 4. The peak electron density of $\sim 3 \times 10^{24}$ 1/cc is lower than in most plastic implosions on Omega because the implosion was designed to be at lower compression and more stable. Measurements based on monochromatic differential imaging[18,19] of core x rays are planned to infer the time-resolved evolution of D_2-core profiles in the near future, using techniques similar to those described elsewhere.[20]

IV. CONCLUSIONS

The compressed-core, electron temperature-density profiles of a cryogenic deuterium (D_2) target have been characterized using the measured primary DD and secondary DT yields, neutron-averaged ion temperature, and core x-ray images at peak neutron production. The inferred temperature-density profiles are in good agreement with predictions of the 1D hydrocode LILAC. The electron pressure and burn and triton-stopping region ρR's were inferred to be 2.7 ± 0.4 Gbar, ~ 10 mg/cm^2, and ~ 23 mg/cm^2, respectively. This work introduces a more accurate hot-core characterization from previous techniques. The modeling, presented in this paper, is based on 1D core profiles: it could be extended to full 3D modeling of less homogenous implosions with the addition of multiview, tomographic imaging.

[1] J. Nuckolls, L. Wood, A. Thiessen, and G. Zimmerman, Nature (London) **239**, 139 (1972).
[2] J. D. Lindl, *Inertial Confinement Fusion: The Quest for Ignition and Energy Gain Using Indirect Drive* (Springer, New York, 1998), Chap. 6, p. 61.
[3] P. W. McKenty, V. N. Goncharov, R. P. J. Town, S. Skupsky, R. Betti, and R. L. McCrory, Phys. Plasmas **8**, 2315 (2001).
[4] T. R. Boehly, D. L. Brown, R. S. Craxton, R. L. Keck, J. P. Knauer, J. H. Kelly, T. J. Kessler, S. A. Kumpan, S. J. Loucks, S. A. Letzring, F. J. Marshall, R. L. McCrory, S. F. B. Morse, W. Seka, J. M. Soures, and C. P. Verdon, Opt. Commun. **133**, 495 (1997).
[5] F. J. Marshall, S. A. Letzring, C. P. Verdon, S. Skupsky, R. L. Keck, J. P. Knauer, R. L. Kremens, D. K. Bradley, T. Kessler, J. Delettrez, H. Kim, J. M. Soures, and R. L. McCrory, Phys. Rev. A **40**, 2547 (1989).
[6] Y. Kitagawa, K. A. Tanaka, M. Nakai, T. Yamanaka, K. Nishihara, H. Azechi, N. Miyanaga, T. Norimatsu, T. Kanabe, C. Chen, A. Richard, M. Sato, H. Furukawa, and S. Nakai, Phys. Rev. Lett. **75**, 3130 (1995).
[7] H. Azechi, N. Miyanaga, R. O. Stapf, K. Itoga, H. Nakaishi, M. Yamanaka, H. Shiraga, R. Tsuji, S. Ido, K. Nishihara, Y. Izawa, T. Yamanaka, and C. Yamanaka, Appl. Phys. Lett. **49**, 555 (1986).
[8] M. D. Cable and S. P. Hatchett, J. Appl. Phys. **62**, 2233 (1987).
[9] P. B. Radha, J. Delettrez, R. Epstein, V. Yu. Glebov, R. Keck, R. L. McCrory, P. McKenty, D. D. Meyerhofer, F. Marshall, S. P. Regan, S. Roberts, T. C. Sangster, W. Seka, S. Skupsky, V. Smalyuk, C. Sorce, C. Stoeckl, J. Soures, R. P. J. Town, B. Yaakobi, J. Frenje, C. K. Li, R. Petrasso, F. Séguin, K. Fletcher, S. Padalino, C. Freeman, N. Izumi, R. Lerche, and T. W. Phillips, Phys. Plasmas **9**, 2208 (2002).
[10] S. Kurebayashi, J. A. Frenje, F. H. Séguin, J. R. Rygg, C. K. Li, R. D. Petrasso, V. Yu. Glebov, J. A. Delettrez, T. C. Sangster, D. D. Meyerhofer,

C. Stoeckl, J. M. Soures, P. A. Amendt, S. P. Hatchett, and R. E. Turner, Phys. Plasmas **12**, 032703 (2005).

[11] M. D. Cable, S. P. Hatchett, J. A. Caird, J. D. Kilkenny, H. N. Kornblum, S. M. Lane, C. Laumann, R. A. Lerche, T. J. Murphy, J. Murray, M. B. Nelson, D. W. Phillion, H. Powell, and D. B. Ress, Phys. Rev. Lett. **73**, 2316 (1994).

[12] T. C. Sangster, J. A. Delettrez, R. Epstein, V. Yu. Glebov, V. N. Goncharov, D. R. Harding, J. P. Knauer, R. L. Keck, J. D. Kilkenny, S. J. Loucks, L. D. Lund, R. L. McCrory, P. W. McKenty, F. J. Marshall, D. D. Meyerhofer, S. F. B. Morse, S. P. Regan, P. B. Radha, S. Roberts, W. Seka, S. Skupsky, V. A. Smalyuk, C. Sorce, J. M. Soures, C. Stoeckl, K. Thorp, J. A. Frenje, C. K. Li, R. D. Petrasso, F. H. Séguin, K. A. Fletcher, S. Padalino, C. Freeman, N. Izumi, J. A. Koch, R. A. Lerche, M. J. Moran, T. W. Phillips, and G. J. Schmid, Phys. Plasmas **10**, 1937 (2003).

[13] Y. Lin, T. J. Kessler, and G. N. Lawrence, Opt. Lett. **20**, 764 (1995).

[14] S. P. Regan, J. A. Marozas, J. H. Kelly, T. R. Boehly, W. R. Donaldson, P. A. Jaanimagi, R. L. Keck, T. J. Kessler, D. D. Meyerhofer, W. Seka, S. Skupsky, and V. A. Smalyuk, J. Opt. Soc. Am. B **17**, 1483 (2000).

[15] T. R. Boehly, V. A. Smalyuk, D. D. Meyerhofer, J. P. Knauer, D. K. Bradley, R. S. Craxton, M. J. Guardalben, S. Skupsky, and T. J. Kessler, J. Appl. Phys. **85**, 3444 (1999).

[16] C. K. Li and R. D. Petrasso, Phys. Rev. Lett. **70**, 3059 (1993).

[17] W. J. Karzas and R. Latter, Astrophys. J., Suppl. **6**, 167 (1961).

[18] J. A. Koch, S. W. Haan, and R. C. Mancini, J. Quant. Spectrosc. Radiat. Transf. **88**, 433 (2004).

[19] V. A. Smalyuk, V. N. Goncharov, J. A. Delettrez, F. J. Marshall, D. D. Meyerhofer, S. P. Regan, and B. Yaakobi, Phys. Rev. Lett. **87**, 155002 (2001).

[20] I. Golovkin, R. Mancini, S. Louis, Y. Ochi, K. Fujita, H. Nishimura, H. Shirga, N. Miyanaga, H. Azechi, R. Butzbach, I. Uschmann, E. Förster, J. Delettrez, J. Koch, R. W. Lee, and L. Klein, Phys. Rev. Lett. **88**, 045002 (2002).